Highly Intelligent Forward Design of Metamaterials Empowered by Circuit-Physics-Driven Deep Learning

*Yiming Yan[#], Fajun Li[#], Jiaqing Shen, Mingyong Zhuang, Yuan Gao, Wei Chen, Yuyang Li, Zhilin Wu, Zhaogang Dong, Jinfeng Zhu**

Y. Yan, F. Li, J. Shen, Y. Gao, W. Chen, Y. Li, M. Zhuang, Z. Wu, Prof. J. Zhu
Institute of Electromagnetics and Acoustics and Key Laboratory of Electromagnetic Wave Science and Detection Technology, Xiamen University, Xiamen, Fujian 361005, China
# These authors contributed equally. *E-mail: nanoantenna@hotmail.com

Prof. Z. Dong

Institute of Materials Research and Engineering (IMRE), Agency for Science, Technology and Research (A*STAR) , 2 Fusionopolis Way, Innovis #08-03, Singapore 138634, Republic of Singapore

Keywords: Deep learning, Physics-informed, Generalization, Optical design, Metamaterials

The field of advanced metamaterial design has witnessed the great progress of artificial intelligence (AI) for science. Typically, the widely used deep learning is a purely data-driven approach. However, it is often assumed as a black box performing interpolation among training data in a fuzzy way, which suffers from poor generalization outside the training domain of critical physical parameters. Inspired by physics-guided deep learning, a circuit-theory-informed neural network (CTINN) in order to strengthen the generalization of metamaterial design is proposed. A series of plasmonic stack metamaterials (PSMs) are taken as learning paradigms of CTINN. Compared to conventional deep learning, the scheme decreases one-order lower test loss of spectral prediction beyond the structure training span, and it possesses an extraordinary function to predict spectra of the extrapolated wavelength range. Due to the physics-informed mechanism, the CTINN only adopts 10% training samples of the pure data-

driven counterpart, while it reduces >50% test loss. Moreover, the CTINN design is used to guide the PSM experiments and demonstrate its great potential for metamaterial development. This work introduces the theory of equivalent circuits into the neural network, empowers physics supervision to AI, and accomplishes the smart and powerful design of PSMs.

1. Introduction

Nowadays, the concept of metamaterials has become a powerful tool in the fields of nanophotonics and optical engineering, since they can be flexibly designed to manipulate electromagnetic waves at the nanoscale.[1–8] Conventionally, the design of metamaterials typically depends on a lot of optical simulation and rich research experiences. Along with the fast development of artificial intelligence, deep learning (DL) based on artificial neural network (NN) has brought about great advancements on metamaterials design. Many DL models have been reported to boost the design performance of metamaterials, such as multilayer perceptron (MLP), convolutional NN, generative adversarial network, transformer and so on.[9–16] These models are based on the data-driven approach, and have a capability to establish the correlation between metamaterial structures and optical responses. The trained NN supports the spectrum prediction according to a given metamaterial structure within milliseconds, which has the overwhelming advantage compared to the time-consuming simulation in conventional design. However, the NN is often used as a black box performing interpolation among training data without basic physical insight.[17,18] Such NN predicts the optical spectra of metamaterials in a fuzzy way, and suffers from poor generalization outside the training domain, which is easy to induce inaccurate or even physically implausible prediction during the design process. Thus, there is still impending demand of introducing essential physical mechanism to enhance the NN generalization for precise metamaterial design.

On the other hand, since the conceptual birth of optical metamaterials, many physical theories have been developed to explain or aid their design.[19–23] Among these theories, the physics of optical nanocircuit proposed by the metamaterial pioneer Nader Engheta has attracted great interest.[24–27] This is because it analyzes meta-atoms as equivalent resistor-inductor-capacitor (RLC) circuits, which provides an eyesight via existing knowledge of microwave electronics to interpret optical spectra of metamaterials qualitatively.[28–30] However, its applications on quantitative design of metamaterials are still hindered due to difficulties in extracting explicit

circuit parameters, especially the optical nanocircuit theory based on artificial learning architectures.

In this study, we develop a design model based on the circuit-theory-informed neural network (CTINN), which incorporates prior physical insights[31–35] extracted from equivalent RLC circuits into the DL approach as illuminated in **Figure 1**. In order to demonstrate the effectiveness of proposed approach, we take the design of plasmonic stack metamaterial (PSM) as a paradigm, which consist of metal/dielectric/metal (MDM) subwavelength unit cells in the infrared range. Compared with the conventional MLP, the CTINN indicates the extraordinary capability of extrapolation on metastructure space with high design precision by using fewer training parameters. The CTINN can predict spectral responses beyond the wavelength range of given data samples, which cannot be achieved by the MLP. Our scheme can also support strong physical generalization of metamaterial design by adopting the small sampling space during data feeding. The proposed NN is endowed with physical intelligence by introducing principles of equivalent circuit, and is believed to inspire more smart design applications of DL on metamaterials.

2. Results and Discussion

2.1. Architecture of CTINN for Metamaterial Design

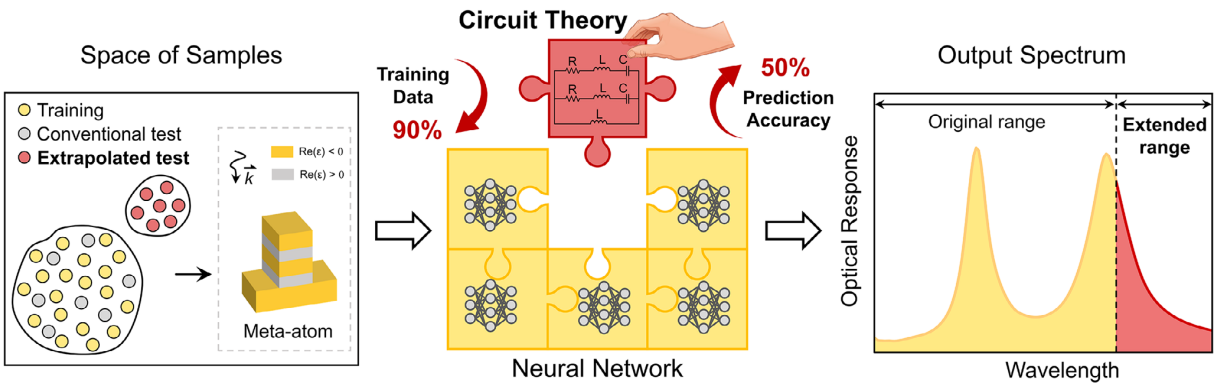

Figure 1. Conceptual diagram of highly intelligent metamaterial design empowered by circuit-physics-driven deep learning.

The framework of CTINN is illustrated in **Figure 2**, which consists of the normalization layer, input layer, fully connected hidden layers, circuit parameters layer, physics-informed operation layer and output spectrum. The sequence $G=\{x_1 \ldots x_i \ldots x_j \ldots x_n\}$ for geometry structure parameters of metamaterial unit cell is fed into the network, and normalized as $G'=\{x'_1 \ldots x'_i \ldots x'_j \ldots x'_n\}$ with each element ranging from 0 to 1, which makes the input data less sensitive to the large-scale variation of metastructure sizes. After the hidden layers, there is the layer for equivalent circuit parameters of metamaterial, including resistors, inductors, capacitors and related tuning factors (R, L, C, T…). We use the Softplus function to confine these parameters to positive values. They are introduced into the physics-informed operation layer based on the circuit function $F(\lambda)$, which is followed by the layer of output spectrum. The loss function of CTINN is defined as the mean square error (MSE) between the predicted results and simulated ground truth by rigorous coupled wave analysis (RCWA),[36] and it is expressed as below:[15]

$$\text{Loss} = \frac{1}{N}\sum_{i=1}^{N}(S'_i - S_i)^2 \qquad (1)$$

where S'_i and S_i denote the predicted and simulated spectrum, respectively and N is the number of spectral sampling points.

The entire network adopts ReLU[37] as the activation function, and use the Adam as the gradient descent optimizer,[38] which has been proven to be a powerful optimizer of DL. Aided by the circuit theory, the CTINN is mainly developed to enhance physical generalization of metamaterial design from two aspects, as indicated in Figure 1. On one hand, the network can be used to predict spectra for tested metastructure sizes beyond the trained numerical ranges of x_1, …, x_i, …, x_j and x_n. On the other hand, the network can be used to extend the predicted spectrum range outside the trained wavelength span. With the aim to evaluate the generalization capability of CTINN, we next focus on using it to design some classical metamaterial instances, such as PSM with the meta-atoms of one MDM stack and double MDM stacks.

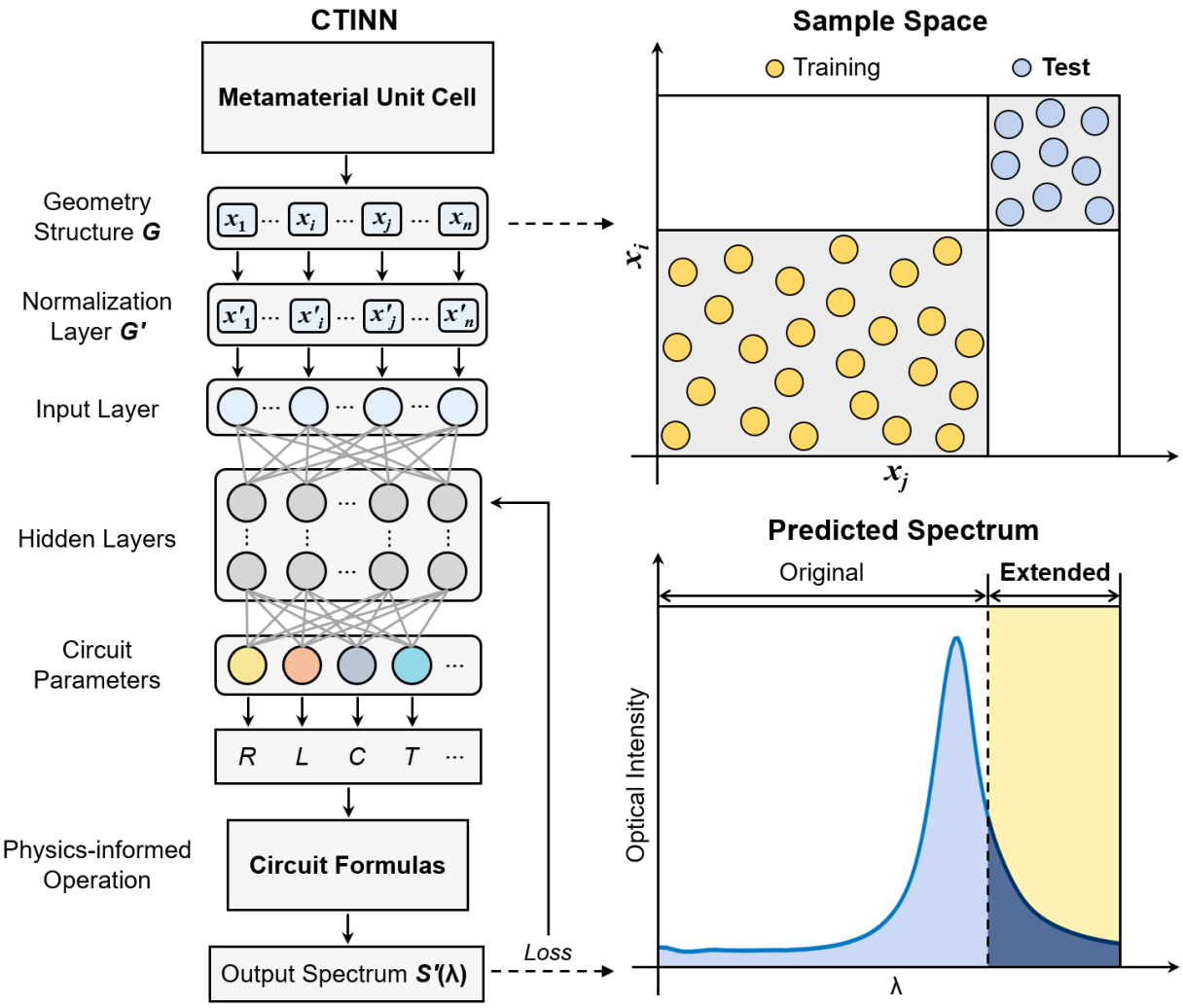

Figure 2. Schematic drawing of CTINN with the circuit-theory-derived capability of generalization for metamaterial design.

2.2. Design and Fabrication Guide for PSMs with Meta-atoms of Single MDM Stack

The configuration of MDM stack can be assumed as a common component of metamaterials, and it is widely used to design various meta-atoms, especially for applications on light trapping, energy harvest and optical sensing.[39–44] The schematic drawing of a plasmonic metamaterial with subwavelength MDM stacks are shown in **Figure 2a**. When a transverse magnetic wave is vertically incident on the PSM, the physical model of MDM meta-atom can be described by the equivalent RLC circuit. The current of the critical RLC branch can be expressed as below:[29]

$$I = \frac{j\omega C V_0}{1 + j\omega CR - \omega^2 LC} \quad (2)$$

where V_0, R, C and ω represent the source voltage, resistance, capacitance and angular frequency, respectively; L is the inductance including the dynamic and Faraday parts induced

by the electron drift and mutual interaction of two metal stacks; L_∞ and C_A denote the infinitely-great inductance of bottom metal layer and infinitesimal capacitance upon the meta-atom.

Based on the equivalent circuit, the spectral absorbance of meta-atom could be referred to the resistance loss in the RLC branch. This facilitates a better understanding of PSM optical response from the perspective of circuit theory. Despite of given metastructure sizes, one usually fails to calculate the definite values for the set of equivalent RLC parameters without obtaining the corresponding spectrum in advance[29]. In fact, the circuit-based optical response should be fitted by a series of trial-and-error factors according to Equation (2). Thus, we introduce the tuning factors T_1 and T_2 into Equation (2) as below (see more details in Supporting Information):

$$S'(\lambda) = \left| T_1 + T_2 \left| \frac{j2\pi c_0 C V_0}{\lambda^2 + j2\pi c_0 C R\lambda - 4\pi^2 {c_0}^2 LC} \right| \right|^2 R \tag{2}$$

where λ represents the wavelength, $S'(\lambda)$ is the wavelength-dependent output spectrum, c_0 is the velocity of light in vacuum. T_1 and T_2 facilitate flexible spectral fitting in combination with the DL model of CTINN. During the training process, the circuit-based factors R, L, C, T_1 and T_2 are assumed as the automatic fitting parameters of DL.

In order to verify the physical generalization of CTINN, we preliminarily take the classical MDM model as a paradigm, which contains the geometrical parameters, including the period p, width of stack w, thickness of metal stack t_m, thickness of dielectric stack t_d and height of metal substrate h. In order to simplify the model, we fix p at 1000 nm, and make both h and t_m optically thick (≥100 nm).

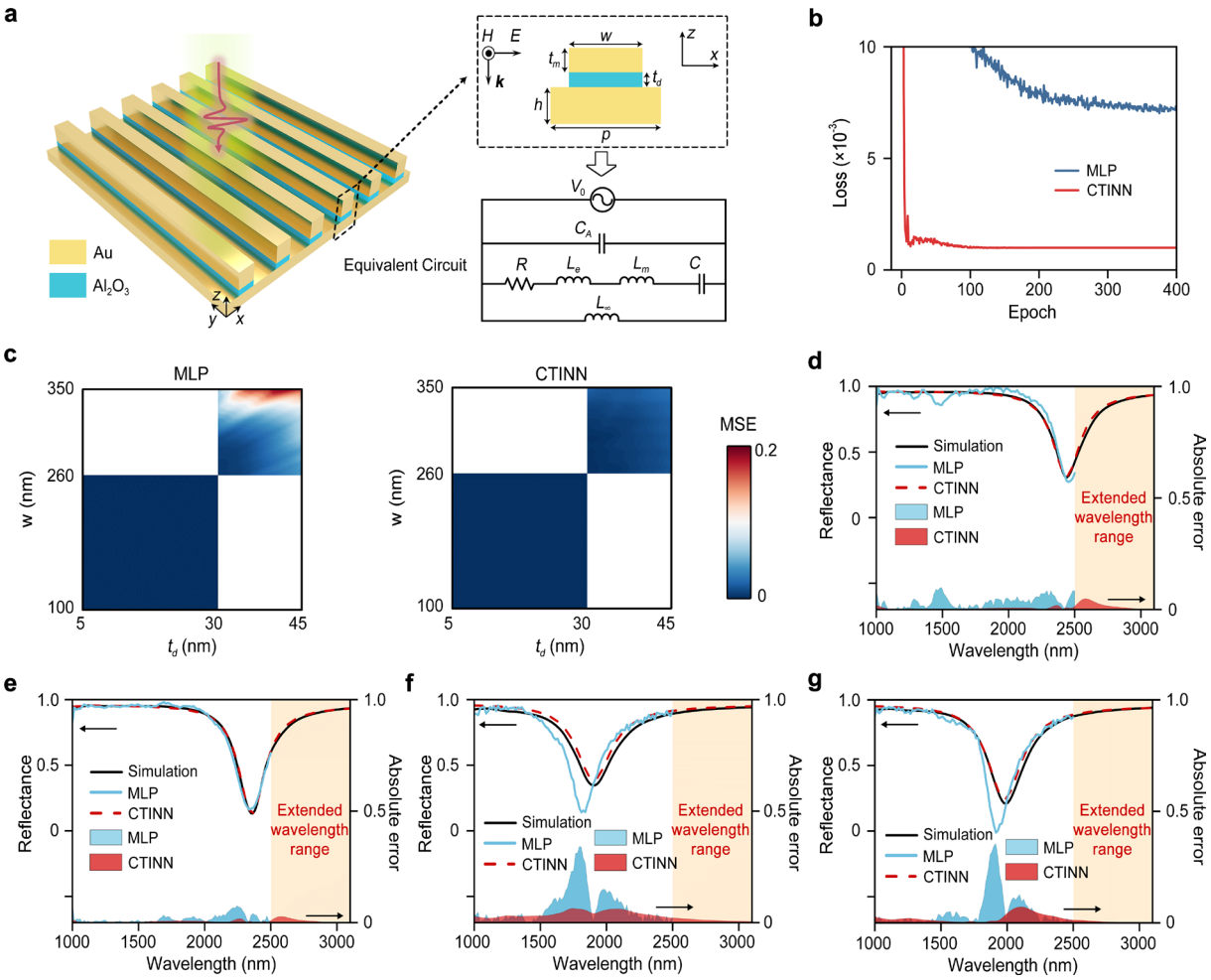

Figure 3. Design generalization of sample space and wavelength range for PSM with meta-atoms of single MDM stack. (a) Schematic drawing of the PSM and the corresponding equivalent RLC circuit. (b) Comparison of test loss between the MLP and CTINN models. (c) MSE heat maps of training and test sets for the MLP and CTINN models. Training instances (d), (e) and test instances (f), (g), which contain simulated spectra and spectra of MLP and CTINN predictions with absolute errors. Only the CTINN can predict spectrum of extended wavelength range in the shadow area.

Initially, we evaluate the design function for extending value span of the geometry parameters $G = [w, t_d]$. We confine the wavelength range of all data samples from 1000 nm to 2500 nm, use 4000 data samples in the range of 100 nm $\leq w \leq$ 259 nm and 5 nm $\leq t_d \leq$ 29 nm as the training set, and adopt 1456 instances in the range of 260 nm $\leq w \leq$ 350 nm and 30 nm $\leq t_d \leq$ 45 nm as the test set, which is apparently outside the training value span. Compared to the classical MLP model, the CTINN with less training parameters (see more details in Figure S1

and Table S1) converges much faster, and the test loss dramatically decreases to a much lower level within several initial epochs, as observed in Figure 3b. The test loss can be as low as 1.0×10^{-3} after 100 epochs, which has a reduction of 85.5% versus the converged value of MLP after 400 epochs.

We further compare the CTINN with the MLP on prediction performance of test set in Figure 3c. As the sizes of w and t_d deviate from the training value span, the MSE in the MLP model increases significantly. In contrast, the CTINN can consistently keep a low level of MSE in the test set, which is still comparable to that in the training set. In fact, about 90% of samples in the MLP model have the MSE larger than 1×10^{-3}, while the CTINN supports over 52% of samples with the MSE less than 1.0×10^{-3} (see more details in Figure S2). The fast convergence and low prediction error of CTINN in the test set could be attributed to the circuit-aided training process. The circuit theory provides physical constraint in the DL model, which transforms the prediction problem for 101 spectral sampling points to that for only 5 circuit-based parameters. This reduces the solution target into the space with a much smaller dimension and lowers the computational complexity greatly. The CTINN can quickly acquire critical data features via the universal physical principle instead of brute-force data feeding, which leads to the high-precision prediction for the PSM design beyond the training value domain.

We continue to analyze design performance by randomly selected training and test instances of CTINN from Figure 3d to Figure 3g. The spectra by the simulated ground truth, MLP are exhibited as the comparison. In the wavelength range from 1000 nm to 2500 nm, the test samples in Figure 3d and 3e exhibit much larger spectral errors than the training samples in Figure 3f and 3g for the MLP model, especially around corresponding plasmonic resonance dips; while the test samples maintain high design accuracy close to the training samples for the CTINN model, generally across the entire spectral band. Moreover, both the training and test instances in the CTINN design display the capability to predict spectra in the extended wavelength range from 2500 nm to 3100 nm, which is not possessed by the MLP model. Based on the statistical analysis of test set, the MSE for the extrapolated wavelength range is as low as 7.1×10^{-5}, which evinces the strong physical generalization for working wavelength extension. This extraordinary design function can be also attributed to the circuit-informed learning

mechanism, in which the CTINN can learn distinct circuit features based on Equation (3) and calculate wavelength-dependent spectra according to the universality of circuit theory.

The intelligent design by CTINN can be also used to guide the experiments of PSM. According to the physics-informed design, we fabricate two different PSM samples by evaporation of multiple thin films and focus ion beam (FIB) lithography, as shown in the scanning electron microscope (SEM) images of **Figure 4**. The SEM images exhibit the uniform periodic PSM meta-atoms with two distinct sets of stack width and dielectric thickness. Figure 4c and Figure 4f show that the measured optical spectra demonstrate good agreement with the predicted spectra by using the CTINN. This indicates that the circuit-theory-informed DL can be effectively adopted to conduct the design and fabrication of PSM with various optical functions, such as narrow-band light absorption and broadband high reflection (see more details in Figure S3). The slight spectral differences between experiments and CTINN design might be attributed to tolerances of nanoscale fabrication or variations of material optical properties, which could be further improved by adopting experimental training data in the near future. Overall, the above results imply the great potential of CTINN design on directing metamaterial experiments.

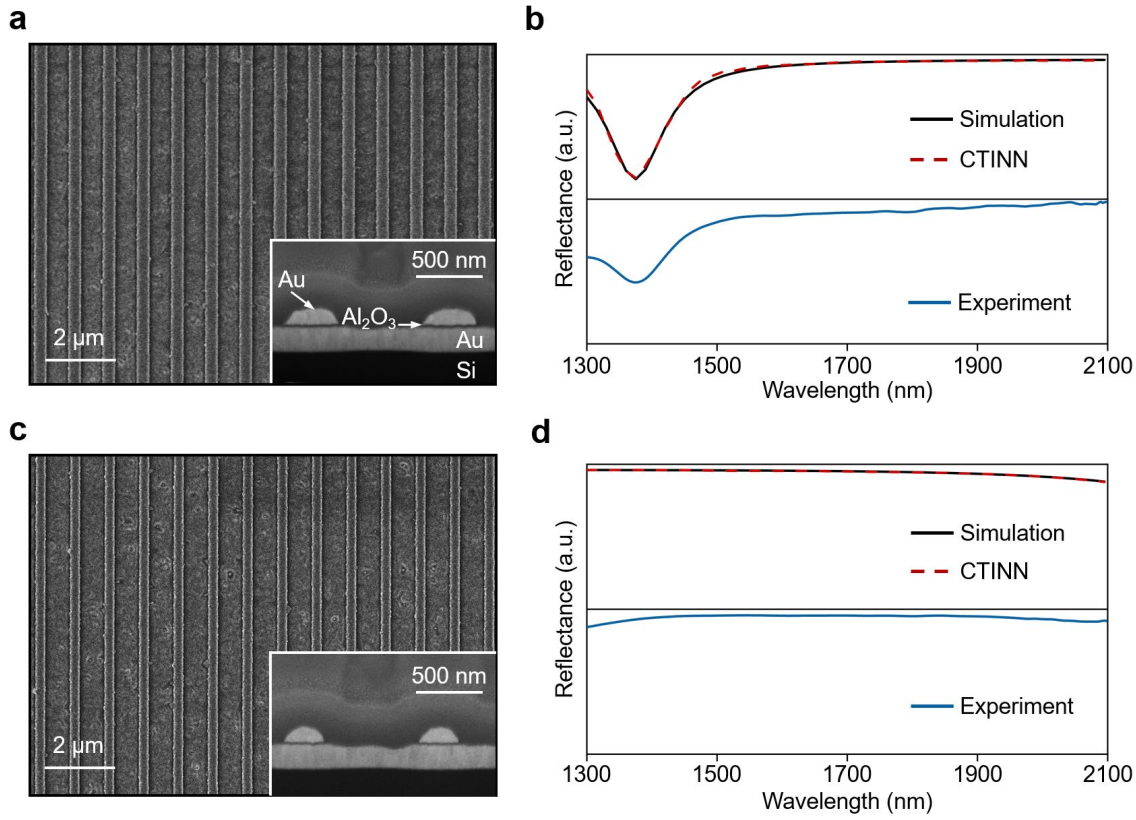

Figure 4. Fabrication guide for two PSMs with meta-atoms of single MDM stack. (a) and (c) are the top-view and cross-section-view (inset) SEM images of the two PSMs, which indicate distinct grating bottom edge lengths of 500nm and 360nm, respectively; (b) and (d) are their measured reflectance spectra in comparison with simulation results and CTINN predictions, respectively.

2.3. Smart Design for Plasmonic Metamaterials with Meta-atoms of Double MDM Stacks

We next extend the CTINN design method for PSMs consisting of subwavelength stacks with more MDM layers. Here, we adopt two typical PSM examples (Type A and B), which contain the meta-atoms with two separate MDM stacks and the meta-atoms of metal/dielectric/metal/dielectric/metal (MDMDM) stack, respectively, as showsn in **Figure 5a**. Both the two meta-atom types consist of the elementary MDM components. According to the circuit theory in Section 2.2, each MDM stack component can be equivalent to an RLC branch. Both the two PSM structures can be described by the same circuit with double RLC branches, as drawn in Figure 5a. In the equivalent circuit, the two MDM-based RLC branches (Branch 1 and Branch 2) are parallel to each other. The whole-circuit meta-atom response of Type A is plotted in Figure 5b. It can be decomposed to two reflectance spectra with plasmonic resonance

dips from the two equivalences of Branch 1 and Branch 2, respectively, which correspond to two single MDM stacks with the gap modes shown in the field distributions. Similarly, the whole-circuit reflectance spectrum for the meta-atom of Type B in Figure 5c is approximately equal to the spectral superposition of two equivalent RLC branches, as illuminated by the corresponding field distributions of single-MDM gap modes. Therefore, we can implement the analogic training mechanism like Section 2.2 to design the two typical PSMs by using the equivalent circuit in Figure 5a.

Here, we adopt the following circuit formula for CTINN:

$$S'(\lambda) = \left| T_{11} + T_{12} \left| \frac{j2\pi c_0 C_1 V_0}{\lambda^2 + j2\pi c_0 C_1 R_1 \lambda - 4\pi^2 c_0{}^2 L_1 C_1} \right| \right|^2 R_1 + \left| T_{21} + T_{22} \left| \frac{j2\pi c_0 C_2 V_0}{\lambda^2 + j2\pi c_0 C_2 R_2 \lambda - 4\pi^2 c_0{}^2 L_2 C_2} \right| \right|^2 R_2 \quad (4)$$

where the two sets of parameters R_1, L_1, C_1 and R_2, L_2, C_2 denote the RLC lumped elements of Branch 1 and Branch 2, respectively. T_{11}, T_{12} and T_{21}, T_{22} represent circuit tuning factors corresponding to these two RLC branches, respectively. During the DL process (see more details in Figure S4 of Supporting Information), the meta-atoms of Type A and B can adopt the same circuit, while their input geometry parameters are entirely different, namely G_A = [w_{A1}, w_{A2}, t_1, t_2] and G_B = [w_B, h_1, h_2, h_3, h_4] provided in Figure 5a.

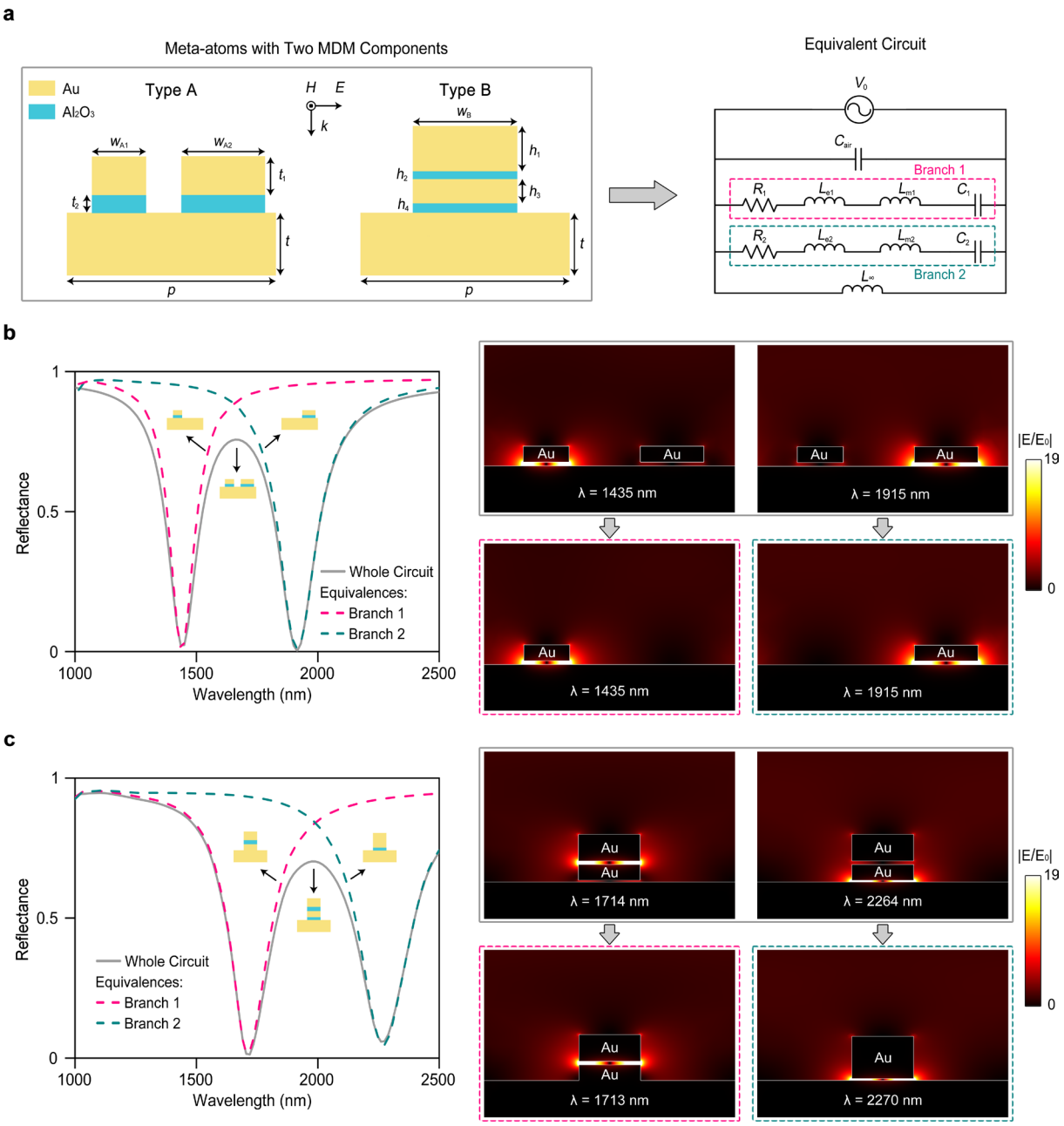

Figure 5. Physical insight of PSMs with meta-atoms of double MDM stacks. (a) Side views of Type A and Type B meta-atoms, whose equivalent RLC circuit contains two main parallel branches. Simulated reflectance spectra of the whole structure and two separate MDM components along with corresponding field distributions at resonance wavelengths for PSMs of (b) Type A and (c) Type B, respectively.

In view of the distinct vector dimensions, we randomly generate 19000 and 30000 samples for their NNs, respectively. We confine the value ranges of 150 nm$\leq w_{A1} \leq$ 250 nm and 250 nm$< w_{A1} \leq$ 300 nm for the training and test data sets of Type A, respectively; while the training and test sets of Type B are in the spans of 150 nm$\leq w_B \leq$ 255 nm and 255 nm$< w_B \leq$ 300 nm, respectively (see other structure parameters in Supporting Information). Obviously, these two test spaces are valued outside the training spans in order to evaluate the geometry generalization. Compared with the conventional MLP, the CTINN demonstrates the test loss of one-order magnitude lower for both the two meta-atom types, as observed in **Figure 5a** (see more details in Figure S5 of Supporting Information).

In fact, the CTINN can keep a much lower level of MSE than the classical MLP model at geometry parameter ranges outside training spans for both Type A and B, which can be observed in Figure 5b. We further exhibit the meta-atom design performance of Type A and B by randomly selecting 6 test instances from Figure 5c to Figure 5h. The MLP spectral prediction of test samples not only lacks the function of wavelength extrapolation, but also shows significant deviations from the simulated ground truth, and the broadband spectral error levels are obviously much higher than the single-MDM meta-atoms shown in Figure 2f and Figure 2g; there are even some optical reflectance values lower than 0 or greater than 100% in the MLP design, which are physically implausible. In contrast, the CTINN predicts the additional spectral range from 2500 nm to 3100 nm for all the samples, and it outputs each spectrum result very close to the ground-truth simulation with much lower absolute errors in the entire wavelength range from 1000 nm to 3100 nm.

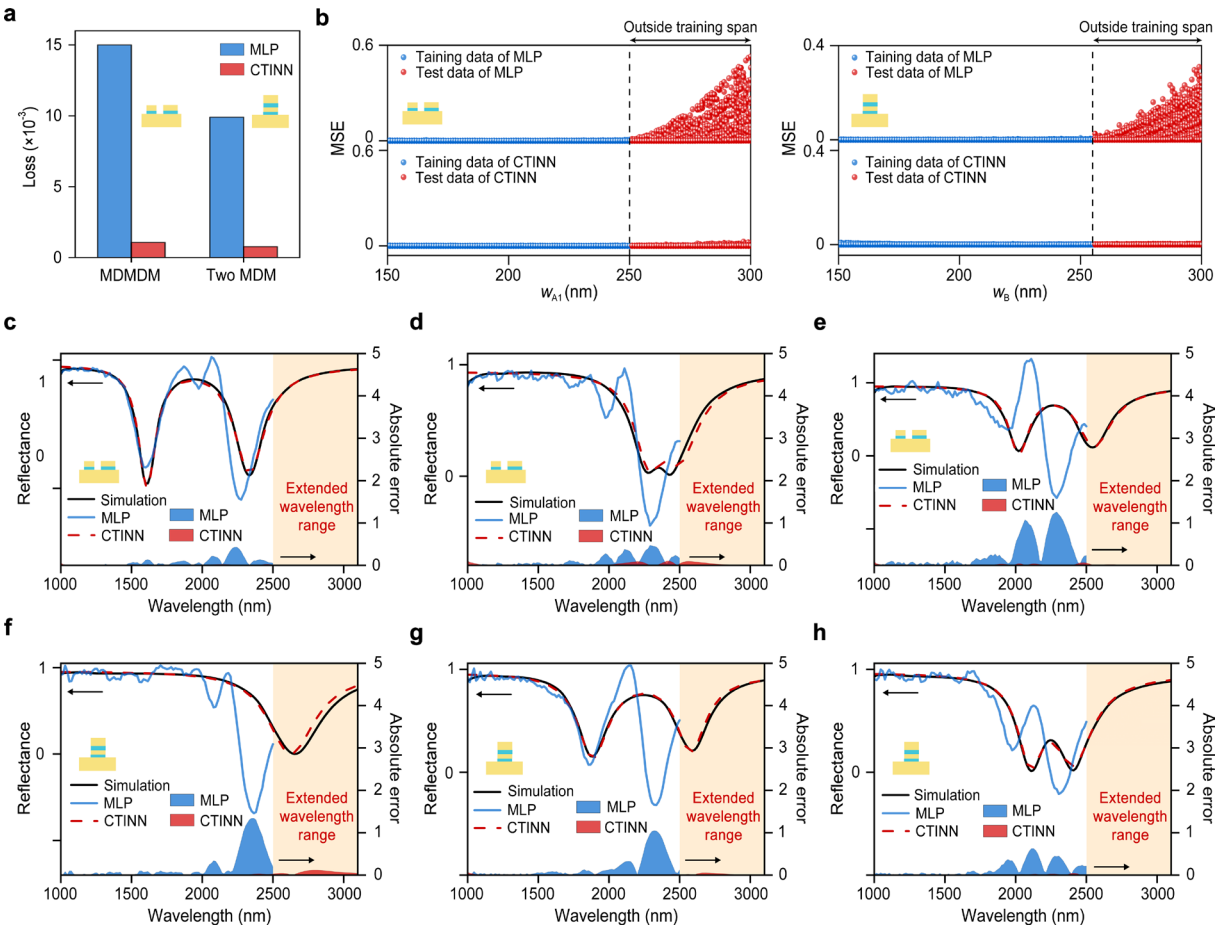

Figure 6. Design generalization of sample space and wavelength range for PSMs with meta-atoms of double MDM stacks. (a) CTINN test loss compared with the MLP for Type A and B. (b) Sample MSE distributions of MLP and the CTINN for Type A and B. Test instances (c), (d), (e) of Type A and test instances (f), (g), (h) of Type B, which contain simulated spectra and spectra of MLP and CTINN predictions with absolute errors. Only the CTINN can predict spectrum of extended wavelength range in the shadow area.

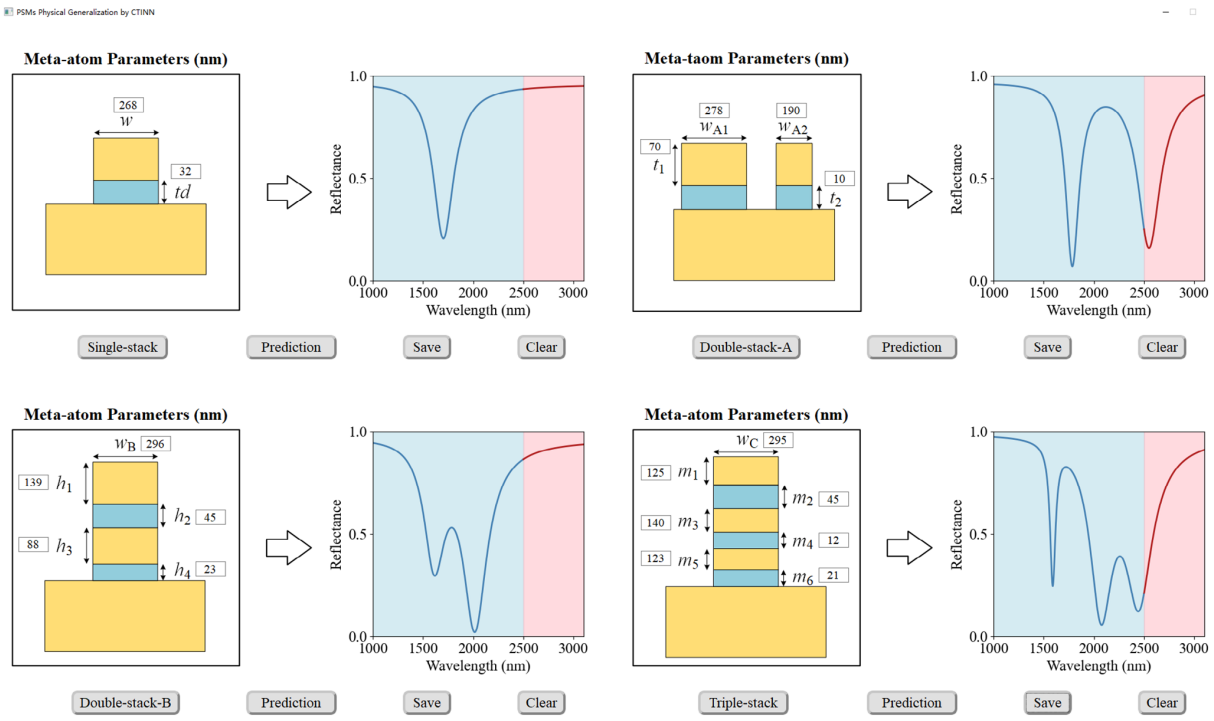

Figure 7. Software platform based on CTINN for universal design of four metamaterial types.

The double-MDM meta-atoms have the higher complexity of geometry structure and equivalent circuit than the single-MDM meta-atoms, but their design still exhibits the low MSE level with strong design generalization, especially for the structure size outside the training span. This should be attributed to the circuit theory learning instead of pure data-driven training. Such learning establishes a one-to-one mapping between structure parameters and circuit-based factors, and empowers a deep insight into the metamaterial physics. The specific learning mechanism ensures the high prediction precision, even for more complex metastructures. Such superior learning approach can be further confirmed by testing the design of PSM with triple-MDM meta-atoms (see Figure S6 in Supporting Information), where the CTINN reduces 82.8% test loss compared to the MLP. Particularly, the physics-informed learning can also decrease the requirement of data sample number dramatically, as shown in **Table 1**. In the double-MDM design case of Type B, the CTINN only adopts 10% training samples of the MLP model, but it

reduces 50.8% loss in the 2000 test samples. Therefore, the CTINN is endowed with strong generalization features, by which it can smartly design high-complexity metamaterials by using very few training samples.

Table 1. Data Requirement and Test Performance

Method	Training Sample Number	Sample Reduction	Test Loss	Loss Reduction
MLP	20000	/	6.1×10^{-3}	/
CTINN	2000	90%	3.0×10^{-3}	50.8%

3. Conclusion

In summary, we propose a neural network based on equivalent circuit theory for the strong generalization of PSM design. By using a small sampling space, it can learn physical relations between input PSM geometry parameters and circuit-based factors during the training process. Our scheme shows superior prediction precision of spectra beyond the structure training span, and it can be also used to extrapolate optical responses in extended wavelength ranges. The physics-informed learning method is used to support the PSM sample fabrication, and the corresponding experimental results exhibit good agreement with the smart design. In the near future, one could develop more physics-based deep learning models and explore extensive design of metamaterials and metadevices.

4. Experimental Section

Fabrication, characterization and measurement: The preparation process is provided in Figure S7 of Supporting Information. Initially, a 5 nm chromium and 150 nm gold layer are deposited onto a 1×1 cm silicon substrate using magnetron sputtering at a rate of 10 Å/s (DISC-SP-3200, Beijing Chuangshiweina Technology Co., Ltd., China). The alumina deposition is next employed using the atomic layer deposition (ALD) at a rate of 0.1 nm per layer (TFS-200-PEALD, Beneq, Finland). Subsequently, the second gold layer of 100 nm thick is deposited onto the substrate using magnetron sputtering. After this, a 40×40 μm nanoarray is etched using FIB (Crossbeam 540, Carl Zeiss, Germany) in accordance with the predefined layout. Finally,

the morphologies are characterized by the FIB system. In the cross-section characterization, we evaporate platinum of 300 nm thick on the PSM surface in order to protect the topography of nanostructure. The reflectance spectra of PSM samples are measured by the UV-Visible-NIR microspectrophotometer (CRAIC 20/30PV, CRAIC Technologies Inc., America), and the results of each spectrum line are based on the average of 25 measurement runs.

Numerical simulation and data collection: Numerical simulation performed with the RCWA and finite element method based on Comsol Multiphysics. In the optical simulation, Floquet boundary conditions are applied on infinite meta-atoms of each PSM. The metamaterial model is discretized by adaptive inhomogeneous triangle meshing, while the minimum edge length of mesh element is as small as 0.044 nm for high convergence and reproducibility of simulation. The materials of metal and dielectric are gold (Au)and alumina (Al_2O_3), respectively. Al_2O_3 is assumed to be nonmagnetic and lossless with the refractive index of 1.74. [1] The dispersive optical parameters of gold are obtained from the literature. [2] The thicknesses of all the gold stacks are greater than the skin depth. The period of meta-atom and height of gold substrate are all fixed at 1000 nm and 200nm, respectively. All data samples are generated by using a desktop (Windows10 operation system, GeForce GTX 3060Ti GPU, Intel(R) Core(TM) i7-9700 CPU @ 3.00 GHz and 16GB of RAM). Both the MLP and CTINN models are built based on the open-source machine learning framework of PyTorch. The software version is Python3.7.

Supporting Information

Supporting Information is available from the Wiley Online Library or from the author.

Acknowledgements

This work was supported by xxx (). The authors thank engineer Yuan Cheng from Instrumentation and Service Center for Molecular Sciences at Westlake University for the assistance of reflectance spectrum measurement and data interpretation. Z.D.

would like to acknowledge the funding support from the Agency for Science, Technology and Research (A*STAR) under its MTC IRG (Project No. M21K2c0116 and M22K2c0088), the Quantum Engineering Programme 2.0 (Award No. NRF2021-QEP2-03-P09) and DELTA-Q 2.0 (Project No. C230917005).

Received:

Revised:

Published online:

References

[1]. N. I. Zheludev, Y. S. Kivshar, *Nature Mater* **2012**, *11*, 917.

[2]. D. Lin, P. Fan, E. Hasman, M. L. Brongersma, *science* **2014**, *345*, 298.

[3]. C. Della Giovampaola, N. Engheta, *Nature materials* **2014**, *13*, 1115.

[4]. W. J. Padilla, R. D. Averitt, *Nat Rev Phys* **2021**, *4*, 85.

[5]. D. Ray, T. V. Raziman, C. Santschi, D. Etezadi, H. Altug, O. J. F. Martin, *Nano Lett.* **2020**, *20*, 8752.

[6]. B. Xiong, Y. Liu, Y. Xu, L. Deng, C.-W. Chen, J.-N. Wang, R. Peng, Y. Lai, Y. Liu, M. Wang, *Science* **2023**, *379*, 294.

[7]. T. Liu, J.-Y. Ou, K. F. MacDonald, N. I. Zheludev, *Nat. Phys.* **2023**, *19*, 986.

[8]. O. Hess, J. B. Pendry, S. A. Maier, R. F. Oulton, J. M. Hamm, K. L. Tsakmakidis, *Nature materials* **2012**, *11*, 573.

[9]. J. Peurifoy, Y. Shen, L. Jing, Y. Yang, F. Cano-Renteria, B. G. DeLacy, J. D. Joannopoulos, M. Tegmark, M. Solja, *SCIENCE ADVANCES* **2018**.

[10]. W. Ma, F. Cheng, Y. Liu, *ACS Nano* **2018**, *12*, 6326.

[11]. D. Liu, Y. Tan, E. Khoram, Z. Yu, *ACS Photonics* **2018**, *5*, 1365.

[12]. Y. Chen, J. Zhu, Y. Xie, N. Feng, Q. H. Liu, *Nanoscale* **2019**, *11*, 9749.

[13]. S. Molesky, Z. Lin, A. Y. Piggott, W. Jin, J. Vucković, A. W. Rodriguez, *Nature Photon* **2018**, *12*, 659.

[14]. J. Xiong, J. Shen, Y. Gao, Y. Chen, J.-Y. Ou, Q. H. Liu, J. Zhu, *Laser & Photonics Reviews* **2023**, *17*, 2100738.

[15]. W. Chen, Y. Gao, Y. Li, Y. Yan, J. Ou, W. Ma, J. Zhu, *Advanced Science* **2023**, *10*, 2206718.

[16]. W. Chen, Y. Li, Y. Liu, Y. Gao, Y. Yan, Z. Dong, J. Zhu, *Advanced Optical Materials* **2024**, *12*, 2301697.

[17]. A.-P. Blanchard-Dionne, O. J. F. Martin, *Opt. Lett.* **2020**, *45*, 2922.

[18]. C. C. Nadell, B. Huang, J. M. Malof, W. J. Padilla, *Opt. Express* **2019**, *27*, 27523.

[19]. D. Stroud, *Phys. Rev. B* **1975**, *12*, 3368.

[20]. J. Homola, M. Piliarik, *Surface plasmon resonance (SPR) sensors*, Springer, **2006**.

[21] F. Liu, X. Zhang, *Biosensors and Bioelectronics* **2015**, *68*, 719.

[22]. M. F. Limonov, M. V. Rybin, A. N. Poddubny, Y. S. Kivshar, *Nature photonics* **2017**, *11*, 543.

[23]. J. Shi, F. Monticone, S. Elias, Y. Wu, D. Ratchford, X. Li, A. Alù, *Nat Commun* **2014**, *5*, 3896.

[24]. N. Engheta, A. Salandrino, A. Alù, *Phys. Rev. Lett.* **2005**, *95*, 095504.

[25] N. Engheta, *Science* **2007**, *317*, 1698.

[26]. A. Alù, N. Engheta, *Phys. Rev. Lett.* **2009**, *103*, 143902.

[27]. H. Caglayan, S.-H. Hong, B. Edwards, C. R. Kagan, N. Engheta, *Phys. Rev. Lett.* **2013**, *111*, 073904.

[28]. T. W. Hughes, S. Fan, *Nano Lett.* **2016**, *16*, 5764.

[29]. J. Zhu, L. Zhang, S. Jiang, J.-Y. Ou, Q. H. Liu, *Nanoscale* **2020**, *12*, 2057.

[30]. T. J. Davis, D. E. Gómez, A. Roberts, *Nanophotonics* **2016**, *6*, 543.

[31]. M. Raissi, P. Perdikaris, G. E. Karniadakis, *Journal of Computational Physics* **2019**, *378*, 686.

[32]. G. E. Karniadakis, I. G. Kevrekidis, L. Lu, P. Perdikaris, S. Wang, L. Yang, *Nat Rev Phys* **2021**, *3*, 422.

[33]. L. G. Wright, T. Onodera, M. M. Stein, T. Wang, D. T. Schachter, Z. Hu, P. L. McMahon, *Nature* **2022**, *601*, 549.

[34]. Y. Liu, W. Liu, X. Yan, S. Guo, C. Zhang, *Journal of Computational Physics* **2023**, *490*, 112291.

[35]. O. Khatib, S. Ren, J. Malof, W. J. Padilla, *Advanced Optical Materials* **2022**, *10*, 2200097.

[36]. V. Liu, S. Fan, *Computer Physics Communications* **2012**, *183*, 2233.

[37]. V. Nair, G. E. Hinton, In Proceedings of the 27th international conference on machine learning (ICML-10), **2010**, pp. 807–814.

[38]. D. Yi, J. Ahn, S. Ji, *APPLIED SCIENCES-BASEL* **2020**, *10*.

[39]. J. Park, K.-Y. Kim, I.-M. Lee, H. Na, S.-Y. Lee, B. Lee, *Opt. Express* **2010**, *18*, 598.

[40]. N. Zhang, K. Liu, Z. Liu, H. Song, X. Zeng, D. Ji, A. Cheney, S. Jiang, Q. Gan, *Advanced Materials Interfaces* **2015**, *2*, 1500142.

[41]. Y. Li, C. Lin, K. Li, C. Chi, B. Huang, *Nano Lett.* **2022**, *22*, 5659.

[42]. T. Shao, X. Wang, H. Dong, S. Liu, D. Duan, Y. Li, P. Song, H. Jiang, Z. Hou, C. Gao, Y. Xiong, *Advanced Materials* **2022**, *34*, 2202367.

[43]. A. V. Kabashin, P. Evans, S. Pastkovsky, W. Hendren, G. A. Wurtz, R. Atkinson, R. Pollard, V. A. Podolskiy, A. V. Zayats, *Nature Mater* **2009**, *8*, 867.

[44]. Y. Hui, J. S. Gomez-Diaz, Z. Qian, A. Alù, M. Rinaldi, *Nat Commun* **2016**, *7*, 11249.